COMMUNICATIONS IN SCIENCE AND TECHNOLOGY
Homepage: cst.kipmi.or.id

Synthesis, characterization and performance of Ni/mesoporous silica - NH_2/mesoporous silica and Ni-NH_2/mesoporous silica as bifunctional catalyst in one step conversion of waste palm oil to biodiesel

Anissa Fitria[a,*], Wega Trisunaryanti[a], Triyono[a], Iman Santoso[b]

[a]*Department of Chemistry, Universitas Gadjah Mada, Yogyakarta 55281, Indonesia*
[b]*Department of Physics, Universitas Gadjah Mada, Yogyakarta 55281, Indonesia*

Article history:
Received: 15 July 2024 / Received in revised form: 16 December 2024 / Accepted: 16 December 2024

Abstract

Sidoarjo mud is a natural material resulted from an unusual natural phenomenon and is rich in silica contents. So far, no studies have been reported about mesoporous silica from Sidoarjo Mud, which is a supported catalyst for one-step conversion to biodiesel. This study aims to explore synthesis, characterization, and applications to demonstrate the heightened activity and selectivity in the esterification- transesterification of waste palm oil into biodiesel, utilizing a one-step method aligned with the principles of green chemistry using two bifunctional catalysts (Ni/MS - NH_2/MS and Ni-NH_2/MS). The bifunctional catalysts were prepared by means of hydrothermal, wet impregnation, and grafting methods. The highest biodiesel yield (78.77%) was achieved under the condition of 65 °C, 3 h, methanol to oil ratio 21 : 1, and 3wt% of Ni/MS - NH_2/MS as the catalyst. The catalyst was able to yield a conversion level as good as ~72% in the 3rd cycle after regeneration. The research demonstrates the industrial relevance of the catalyst, offering a sustainable solution for biodiesel production and waste management.

Keywords: Sidoarjo mud; silica; acid-base bifunctional catalyst; esterification-transesterification; biodiesel

1. Introduction

Petroleum globally has stood as the predominant energy source over recent decades. The finite nature of petroleum reserves, however, is increasingly apparent, exacerbating concerns amidst a continued rise in petroleum consumption annually [1]. Concurrently, the escalating demand for fossil fuels has precipitated a host of challenges, including resource scarcity and environmental degradation [2]. Thus, the imperative is the pursuit of alternative renewable fuels with biodiesel emerging as a particularly promising candidate. Biodiesel, defined as a renewable fuel comprising monoalkyl esters of long-chain fatty acids, shares combustion properties similar to fossil fuels. Particularly, it is biodegradable and non-toxic, offering a viable substitute for conventional fuels [3]. Presently, biodiesel garners significant research interest owing to its environmentally benign nature, minimal air pollution, non-toxicity, heightened efficiency, reduced exhaust emissions, low sulfur content, elevated cetane number, high flash point, biodegradability, and commendable lubrication properties. This fuel can be chemically synthesized by reacting vegetable oil or animal fat with alcohol, typically methanol, yielding a novel chemical compound termed methyl ester, commonly referred to as biodiesel [4].

The commonly utilized raw materials for biodiesel production encompass soybean oil [5], castor oil [6], vegetable oil [7], animal fat [8], and rapeseed oil [9]. However, in light of environmental concerns and considerations regarding the food chain supply [10], employing waste palm oil as a biodiesel feedstock emerges as a viable resolution.

Biodiesel synthesis traditionally uses a two-stage process: first, an acid catalyst used to convert free fatty acids (FFAs) through esterification, and a base catalyst that helps to convert triglycerides through transesterification. This complex production method, however, requires multiple expensive and energy-intensive steps; hence, it leads to a growing interest in a bifunctional catalyst that combines both acid and base functions, allowing for the simultaneous esterification of FFAs and transesterification of triglycerides in a single step [11,12]. This advancement is significant for industry for being potential to reduce production costs [13].

Catalysts with acid-base properties are recognized as bifunctional heterogeneous catalysts [14]. These catalysts are capable of simultaneously performing both esterification and transesterification on FFAs and triglycerides present in oils. The advantages of bifunctional heterogeneous catalysts include their

* Corresponding author.
Email: anissaftr434@gmail.com
https://doi.org/10.21924/cst.9.2.2024.1483

ability to carry out esterification and transesterification processes concurrently, reducing by-product formation, as well as enhancing biodiesel yield [11,15].

Mesoporous silica materials represent a viable catalyst for the production of alternative energy sources, in particular fuels. A pivotal aspect in the synthesis of mesoporous materials lies in the selection of templates [16]. The commonly used templates for mesostructure formation include cationic and neutral surfactants [17]. Notably, cationic surfactants such as CTAB (cetyltrimethylammonium bromide) find frequent application in MCM-41 synthesis, yielding pore diameters typically in the range of 2-4 nm [18,19]. Extensive research has been conducted on the synthesis of mesoporous silica (MS), encompassing prominent materials such as MCM- 41 [20] and SBA-15 [21]. However, much of the silica used is synthetic and does not align with the principles of green chemistry. Therefore, efforts have been focused on developing mesoporous silica using biomass as a sustainable precursor to reduce synthesis costs. Biomass sources rich in silica, such as rice husks, sugarcane bagasse, corn leaves, and bamboo leaves, have then gained attention [22]. This study utilizes Lapindo mud as a source of silica derived from natural materials, which is environmentally friendly and low-cost. In previous contributions, Sidoarjo mud has shown a promise as a material for its high silica content [23]; it contains 56.75% silica compounds and 23.31% alumina [24] showing its potential as the source of silica and alumina, and making it suitable as a raw material for the production of mesoporous silica materials. To enhance acidity, mesoporous silica undergoes metal impregnation via wet impregnation techniques. Moreover, the utilization of Ni metal as a catalyst yields more heightened acidity levels compared to Cr, Cu, and Pd metals [25].

Heterogeneous catalysts exhibit a number of inherent drawbacks, notably the potential for leaching [26]. Leaching can be mitigated by modifying the catalyst to ensure the firm binding of active sites to the carrier. Modifying mesoporous silica catalysts with 3-APTMS to introduce NH_2 groups increases the base sites on the catalyst surface. The presence of Ni/MS and NH_2/MS is poised to enhance the catalytic process's efficiency, effectiveness, and environmental friendliness. Functioning as a bifunctional catalyst, Ni/MS - NH_2/MS operates synergistically, facilitating esterification and transesterification processes in a single step. NH_2 acts as a base catalyst, while Ni metal serves as an acid catalyst, effectively to reduce free fatty acid levels and convert triglycerides into methyl esters, thus promoting greener chemistry.

2. Materials and Methods

2.1. Materials

Materials used for the research included waste palm oil (WPO) from food shop in Yogyakarta, Sidoarjo mud as a source of silica from Sidoarjo, nitrogen gas (N_2), technical hydrogen gas (H_2) from PT. Samator Gas, pro analysis chemicals such as solid $Ni(NO_3)_2 \cdot 6H_2O$, methanol, HCl, NaOH, 37% H_2SO_4 from Merck, 3-aminopropyl trimethoxysilane (3-APTMS) and cetyltrimethylammonium bromide (CTAB) solution from Sigma-Aldrich, distilled water, deionized water, Whatman No. 42 filter paper, and universal pH paper. All chemicals and reagents were of analytical grade.

2.2. Instruments

The extracted solid Sidoarjo mud was analyzed using FTIR (Shimadzu Prestige-21) for functional group identification, XRD (Bruker D8 Advance) for crystal structure analysis, and X-ray Fluorescence (XRF) Bruker S2 PUMA for metal composition determination. The obtained mesoporous silica was then characterized with FTIR functional group, XRD for structural properties, TEM (JEOL JEM-1400) for pore imaging, and Surface Area Analyzer (Quantachrome NovaWin2 1200) to assess surface area, pore volume, and pore diameter. The synthesized Ni/MS was analyzed with XRF for metal content, XRD for structural properties, TEM for imaging, SAA for surface parameters, and NH_3-Temperature Program Desorption (Micromeritrics Chemisorb 2750) for surface acidity. Meanwhile, the NH_2/MS and Ni-NH_2/MS catalysts were tested by means of FTIR for functional groups, XRD for crystallinity, TEM for morphological analysis, SAA for surface area and porosity, NH_3-TPD for acidity, and CO_2-Temperature Program Desorption (Micromeritrics Autochem II 2920) for basicity analysis. Further, the characterization of the biodiesel liquid product was conducted with the aid of Gas Chromatography-Mass Spectroscopy (QP2010S Shimadzu) to analyze the chemical composition and identify compounds in biodiesel, such as fatty acid methyl esters (FAME). The ^1H Nuclear Magnetic Resonance (JNM-ECZR 500 MHz) was used to identify hydrogen groups within the molecular structure of biodiesel, enabling to confirm methyl ester formation and product purity. The ^{13}C Nuclear Magnetic Resonance (JNM-ECZR 500 MHz) functions to analyze carbon groups in the biodiesel molecule, providing detailed information on the compound structure and the presence of methyl esters in the final biodiesel product.

2.3. Extraction of silica from sidoarjo mud

100 g of Sidoarjo mud was dried in an oven at 100°C for 24 hours. Subsequently, the dried mud was pulverized using a mortar and sieved through a 100-mesh sieve. The sieved 100 g portion of Sidoarjo mud was then subjected to reflux with 250 mL of 6M HCl solution at 90°C for 3 hours while being stirred. The resulted solids were collected through centrifugation at 2000 rpm. The solid was dried at 120°C for 3 hours. 60 g of dried solid was refluxed with 300 mL of 6M NaOH for 16 hours at 90°C. The filtrate was subsequently filtered using Buchner with Whatman No. 42 paper to obtain a sodium silicate solution. The solution was added 3M HCl until reaching pH 8. The gel-forming sodium silicate solution was then left for 24 hours, washed with distilled water, and dried in an oven at 100°C for 4 hours.

2.4. Synthesis of mesoporous silica (MS)

Mesoporous silica synthesis was performed via the hydrothermal method. The synthesis of mesoporous silica (MS) by the CTAB template, 5 g of CTAB was mixed with 100 mL of distilled water in a hot plate stirrer at 40°C. The homogenized solution was put on the PET glass. Then, 10 g of silica-extracted Sidoarjo mud (SiO_2 content of 98.90 wt.%) and 200 mL of NaOH 2 M were mixed to form the Na_2SiO_3. CTAB solution

was dripped by Na_2SiO_3 solution bit by bit while the solution was mixed until being homogenized and left for 2 h. The solution was added by HCl 2M to reach pH 10 and then left for 4 h as well. Afterwards, the solution was placed into an autoclave at 100°C for 24 h. The white solid formed was washed with distilled water to make it neutralized. The solid was dried at 100°C for 24 h. The MS was calcined for 5.5 h at 540°C.

2.5. Synthesis of Ni/MS catalyst

Nickel loading on mesoporous silica was performed through the wet impregnation method. The 8 wt.% of Ni metal was loaded into the 10 g of MS by wet impregnation method using a salt precursor of $Ni(NO_3)_2.6H_2O$ and dissolved by 100 mL distilled water. The solution was stirred by a magnetic stirrer at 300 rpm for 24 h. It was continued by evaporating the mixture at 80 °C. The solid was gassed by N_2 and calcined at 500 °C for 3 h. The sample was reduced by H_2 gas (flow rate 20 mL/minute) at 550°C for 4 h.

2.6. Synthesis of NH_2/MS and Ni-NH_2/MS

The modification of mesoporous silica with the addition of 3-aminopropyltrimethoxysilane was conducted with the grafting method. The two catalyst materials: MS and Ni-MS, were grafted with the aminopropyl group using APTMS. 10 grams of MS and Ni-MS were each dispersed in 100 mL toluene solution containing 7.7 mL APTMS at 90ºC for 5 h. The resulted solids were collected through centrifugation at 2000 rpm to be washed one-time using toluene and two times using methanol. The products were then dried in an oven at 80ºC at 24 h.

2.7. One step esterification-transesterification process

The transesterification of WPO was carried out in a round-bottom flask connected with a reflux condenser, immersed in an oil bath. Initially, 10 mL WPO was poured into the flask and heated until reaching the desired temperature. Afterwards, the mixture of methanol and catalyst was added into WPO, whereby the catalyst dosage and methanol to oil molar ratio were varied in the range of 1, 3, 5wt % and 15:1, 18:1 to 21:1, respectively. The reaction was conducted with the constant stirring of 400 rpm for a specified period ranging from 3 h, 5h, 7 h at reaction temperature of 60°C, 65°C, and 70°C. After the reaction, the resulted mixture was transferred in a separating funnel to separate the catalyst, biodiesel, and glycerol. The upper layer was identified as biodiesel and the percentage yield of biodiesel was determined by Eq. (1).

$$YB = \frac{WB \times \% ME}{Wfeed} \times 100\% \quad (1)$$

Description:

YB = Yield of biodiesel
WB = Weight of biodiesel
% ME = GC spectra area of the methyl ester (%)
W_{feed} = Feed weight

The yield of fatty acid methyl ester (FAME yield, %) was analyzed by the Gas Chromatography–Mass Spectrometry. Also, using ^{1}H NMR data, the JCO conversion (C) to non-isolated FAME was determined. The integrals for methoxy and methylene groups (AMe and ACH_2 respectively in Eq. (2)) and ^{13}C NMR are presented as follows.

$$C = 100 \times \frac{2AMe}{3ACH2} \quad (2)$$

C = Percentage conversion of triglycerides to corresponding methyl esters
AMe = Integration value of the methoxy protons of the methyl esters
ACH_2 = Integration value of α-methylene protons

2.8. Catalyst stability

The stability of the bifunctional catalyst was tested by evaluating the reusability. For this purpose, the bifunctional catalysts were used in esterification-transesterification reactions to verify their catalytic performance. For these experiments, the used solid catalyst was separated from the reaction mixture by centrifugation. Then, the catalyst was washed with hexane and washed with methanol. Finally, the catalyst was dried at 100°C for 12 h and the active used catalyst was directly used in repeated reactions under the best resulting conditions of this study.

3. Results and Discussion

3.1. Catalyst characterization

3.1.1. Fourier transform infrared spectroscopy

Fig.. 1 (a) shows the characteristic peaks of Sidoarjo mud sample at the wavenumbers of 472 cm^{-1}, indicating the presence of bending Si-O-Si functional groups, and 986 cm^{-1}, which indicated Si-O-Si stretching asymmetry. Additionally, peaks at 516 cm^{-1} and 3620 cm^{-1} indicated the presence of functional groups for bending Si-O-Al and bending Al-OH, while the absorption peak at 1636 cm^{-1} indicated Si-OH bending. Peaks at 3390 cm^{-1} was indicated as Si-OH stretching functional groups. After the Sidoarjo mud was extracted and printed using CTAB, the disappearance of the CTAB template from Mesoporous Silica could be observed from the infrared spectra. In Fig 1. (b) regarding mesoporous silica before calcination, it was observed that peaks at wavenumbers of 2922 cm^{-1}, 2853 cm^{-1}, and 1489 cm^{-1} appeared, belonging to functional groups in the CTAB surfactant. The peak at 2922 cm^{-1} indicated the asymmetric stretching vibration of CH_2 groups, while the peak at 2853 cm^{-1} indicated the symmetric stretching vibration of CH_2 groups. The peak observed at wavenumber 1489 cm^{-1} represented bending symmetry CH_3 groups of CTAB. In Fig. 1(c), the absence of these three peaks CTAB in the infrared spectra of mesoporous silica after calcination indicated that the CTAB surfactant acting as a template was completely removed during the calcination process. In the NH_2/MS and Ni-NH_2/MS samples, it was observed that the groups present in the 3-APTMS compound could be qualitatively seen at the wavenumbers of 2933 cm^{-1} and 2936 cm^{-1}, indicating the vibrations of CH_2 groups. The vibrations of NH_2 group occurred in the region of 1558 cm^{-1}. In contrast, the vibrations of the C-N group could not be observed in the 1200 cm^{-1} region

for being covered by the vibrations of Si-O-Si at the 1095 cm^{-1} region [18]. These results showed that the SM, Ni/SM and Ni/SM with 3-APTMS have been successfully modified.

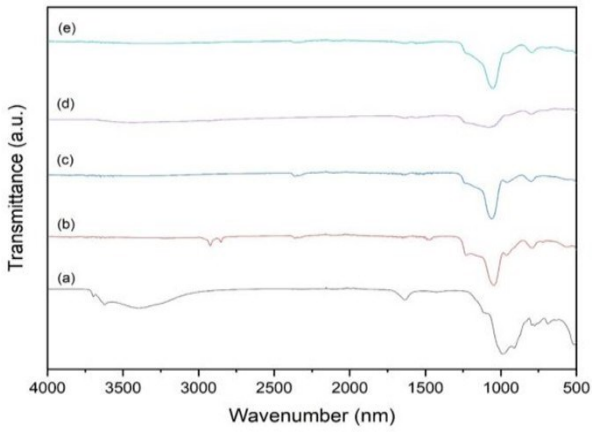

Fig. 1. The FTIR spectra of (a) the Sidoarjo mud, (b) MS Before Calcination, (c) MS After Calcination, (d) NH_2/MS, (e)Ni-NH_2/MS

3.1.2. Fourier transform infrared spectroscopy

Fig. 2. (a) shows the XRD analysis of silica extracted from Sidoarjo mud. A broad peak was observed at 2θ = 22.23°, referring to JCPDS data (card No. 01-086-1561), indicating the characteristics of SiO_2 material and it is amorphous in nature. In Fig. 2. (b), after impregnation with nickel metal, a broad peak with low intensity appeared at 44.53°, consistent with (ICDD 00-045-1027). The broad and weak peak indicates that nickel metal is amorphous. In Fig. 2. (c), the NH_2/MS catalyst was not able to be detected considering that NH_2 (aminopropyl) plays a more significant role as surface functionality, being bound to the silica surface or evenly distributed along the material surface, rather than forming its own crystal structure. Hence, it only showed amorphousness, and did not damage the catalyst structure. Meanwhile, in Fig. 2. (d) the Ni-NH_2/MS catalyst, nickel metal was observed in X-ray diffraction (XRD) with low intensity at 44.52° (ICDD 00-045-1027).

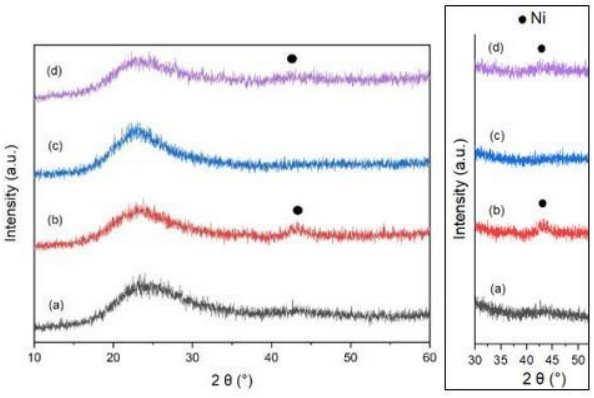

Fig. 2. XRD Diffractogram of (a) MS, (b) Ni/MS, (c) NH2/MS, and (d) Ni-NH_2/MS

3.1.3. Transmission electron microscopy (TEM) analysis

Fig. 3 (a) shows that the synthesized mesoporous silica exhibited a hexagonal-like structure [27] using CTBA as the template. Therefore, it can be stated that the type of template can greatly influences the shape of the resulted mesoporous silica. In Fig. 3 (b) for the Ni/MS catalyst, it was observed that nickel metal in the mesoporous silica support was evenly distributed on the surface, whereas in Fig. 3 (c) for the Ni-NH_2/MS catalyst, it was noticeable that the dispersion of nickel metal was less uniform due to the interaction between NH_2 and nickel metal, causing changes in the structure or partial coverage of the nickel metal surface, which may result in less regular distribution of nickel particles.

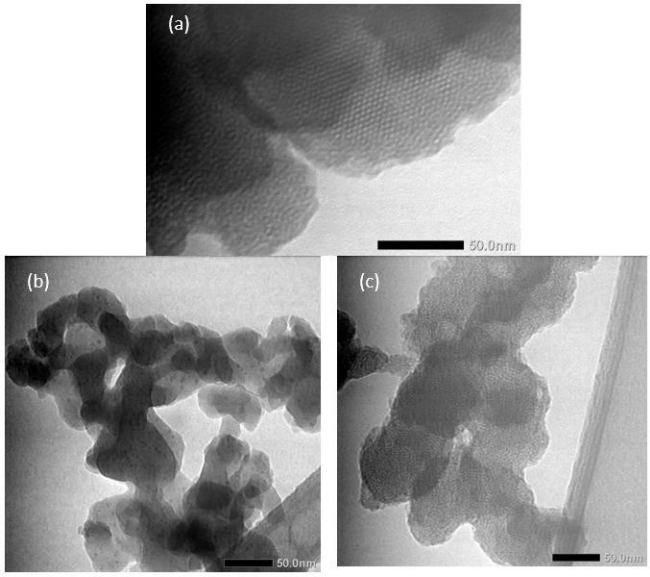

Fig. 3. TEM Images of (a) Mesoporous Silica, (b) Ni/MS, and (c) Ni-NH_2/MS

3.1.4. Surface area analyzer analysis

As shown in Fig. 4 the mesoporous silica and modification mesoporous silica results were demonstrated through Surface Area Analyzer (SAA) analysis, The overall modification of the mesoporous silica catalyst support was classified as type IV according to IUPAC. SAA analysis showed differences in the hysteresis loops among MS, Ni/MS, and Ni- NH_2/MS, indicating a transition from type H_1 in MS to type H_4. Meanwhile, NH_2/MS was classified as type H_2. Table 1 shows the catalyst porosity properties. The rearrangement of the mesoporous silica material followed the micellar structure of the CTAB surfactant, resulting in a high specific surface area. This could enhance the interaction between acidic and basic sites, subsequently added to the mesoporous silica support (MS). The pore characteristics of the catalyst material are crucial for catalytic activity in converting waste palm oil into biodiesel, as they describe an interaction between oil and catalyst. The Ni/MS catalyst experienced a decrease in surface area due to metal covering the pore openings. For the Ni-NH_2/MS catalyst, surface area decreased due to both metal and amino silane covering the mesoporous silica pores. The NH_2/MS catalyst exhibited a significant reduction in surface area with the NH_2 molecules, blocking the pores in the mesoporous silica, confirming successful NH_2 functionalization on the pore walls. The decrease in pore volume in all mesoporous silica-based catalyst modifications was in view of metal distributed on the silica surface and entering the pores, filling or even blocking

some of them. The reduction in pore diameter might also be related to metal adhering to the walls and openings of the mesoporous silica pores.

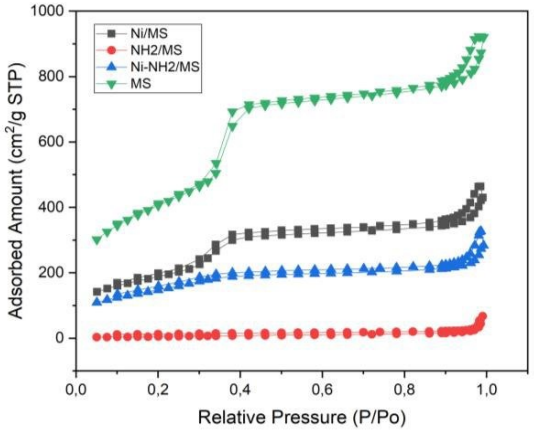

Fig. 4. Isoterm Curve Mesoporous Silica (a) MS, (b) Ni/MS, (c) NH_2/MS, dan (d) Ni-NH_2/MS

Table 1. Catalyst Porosity Properties

Catalyst	Surface Area (m^2g^{-1})	Pore Diameter (nm)	Pore Volume (cm^3g^{-1})
MS	1,452.35	3.87	1.40
Ni/MS	739.71	3.59	0.66
NH_2/MS	21.81	18.45	0.11
Ni-NH_2/MS	540.67	3.20	0.43

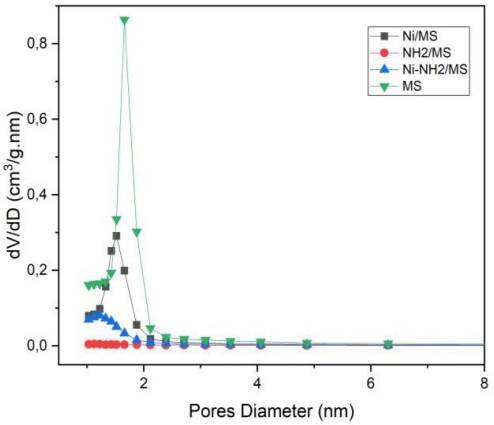

Fig. 5. Pore size distribution

Regarding the pore distribution graph as shown in Fig.5, all the modifications of the mesoporous silica catalysts had the pore size distributions ranging from 1-14 nm. According to IUPAC, pore sizes <2 nm are classified as micropores, while pore sizes in the range of 2 nm to 50 nm are classified as mesopores. As the pore diameter of mesoporous silica was 3.9 nm, it is then classified a mesoporous material, while the Ni/MS, NH_2/MS, and Ni-NH_2/MS catalysts were the combination of microporous and mesoporous materials, dominated by mesopores with the diameters of 2-8 nm. Catalysts with mesoporous sizes have good potential for converting triglycerides, generally sized 2.5 nm, into methyl esters through a one-step esterification- transesterification reaction.

3.1.5. TPD-NH_3 analysis

NH_3-Temperature-programmed desorption (TPD) was used to analyze the total surface acidity using NH_3 as a base probing molecule to provide information about the type and the strength of acid sites of the Ni/MS and Ni-NH_2/MS catalysts. Fig.6 shows the TPD profiles of NH_3. We here focused mainly on the strength of acidity from which NH_3 was desorbed above 350°C as the catalytic evaluation was carried out at high temperatures (751°C) and (585°C). Fig. 6 shows that the Ni/MS catalyst exhibited a single peak around the temperature range of 600-800°C with the highest peak at 751°C, indicating the presence of strong acid sites on the nickel catalyst impregnated on the mesoporous silica catalyst support. Meanwhile, the Ni-NH_2/MS catalyst showed two peaks around 500-800°C with a broader peak compared to Ni/MS, meaning that the Ni-NH_2/MS catalyst had more Brønsted acid sites. However, both catalysts fell within the range of strong acid sites at 350-800°C [28]. The presence of strong acid sites at high temperatures indicated the ability of both Ni/MS and Ni-NH_2/MS catalysts to adsorb and bind NH_3 strongly [29]. Table 2 shows the total acidity value.

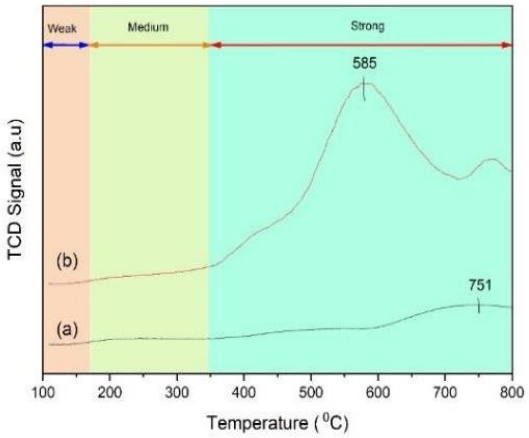

Fig. 6. TPD-NH3 profiles (a) Ni/MS, and (b) Ni-NH_2/MS

Table 2. The amount of NH_3 at desorption peaks linking the acidic sites of the catalysts

Catalyst	Amount of Acidity (mmol g^{-1})
Ni/MS	0.7301
Ni-NH_2/MS	3.2475

3.1.6. TPD-CO_2 analysis

Fig. 7 represents the results of the CO_2-TPD for th e NH_2/MS and the Ni-NH_2/MS catalysts to predict the adsorption effect on the basicity of the catalysts. From the CO_2TPD profile, all catalysts showed three desorption peaks of CO_2. The weak basic site was attributed to the first peak (broad) at a lower temperature of 50–200ºC. While, the medium basic site corresponded to the second peak (broad) from 200°C to 300ºC. The third CO_2 desorption peak (sharp with high TCD signal

intensity) at around 300–800ºC was attributed to the strong basic site [30]. Table 3 shows the total basicity value.

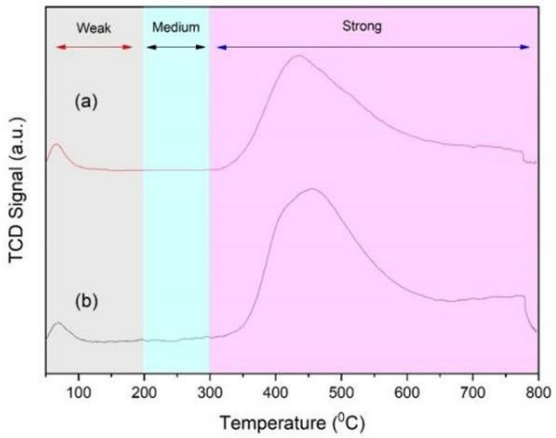

Fig. 7. TPD-CO2 profiles (a) NH2/MS, and (b) Ni-NH2/MS

Table 3. The amount of CO2 at desorption peaks linking the basicity sites on of the catalysts

Catalyst	Amount of Basicity (mmol g^{-1})
NH_2/MS	1.4504
Ni-NH2/MS	2.0890

3.1.7. Base to acid ratio catalyst

TPD-NH_3 and TPD-CO_2 profiles can depict the base- to-acid ratio values obtained as this can significantly impact the biodiesel conversion outcomes. Table 4 shows the total base/acid ratio in which the higher concentrations of bases on bifunctional catalysts are generally preferred to produce methyl esters in the one-step biodiesel production reaction. The optimal base-to-acid ratio with higher base concentrations on bifunctional catalysts can affect the efficiency and outcomes of the reaction [31]. This is because bases act as catalysts in the transesterification reaction as the key step in biodiesel production. With a high base ratio, the number of available base sites will be greater, facilitating more interactions between reactant molecules and enhancing the overall reaction rate. Base catalysts can also assist in breaking glycerol into smaller compounds, increasing reactant conversion, and reducing glycerol formation, thereby enhancing biodiesel yield.

Table 4. Base/acid ratio catalyst

Catalyst	Base/acid ratio
Ni/MS	1.99
Ni-NH_2/MS	0.64

The Ni/MS - NH_2/MS catalyst and Ni-NH_2/MS catalyst exhibited different results. The Ni/MS - NH_2/MS catalyst showed the obtained base-to-acid ratio of 1.99, whereas the one in the Ni-NH_2/MS catalyst was 0.64. The highest base- to-acid ratio was observed in the Ni/MS - NH_2/MS catalyst with a low acidity value of 0.7301 mmol g^{-1} and a doubled basicity value of 1.4504 mmol g^{-1}, resulting in a bifunctional catalyst with a high base-to-acid site ratio. In contrast, the basicity sites found in the Ni-NH_2/MS catalyst were found much lower at 2.0890 mmol g^{-1} compared to its high acidity value of 3.2475 mmol g^{-1}.

3.2. Catalyst activity test

3.2.1. One step esterification-transesterification process using various catalysts

Fig. 8 shows the yield of 44.35% obtained in the Ni-NH_2/MS catalyst. The Ni-NH_2/mesoporous silica catalyst was quite effective in catalyzing esterification- transesterification reactions in a one-step process without undergoing saponification although the conversion yield was not as high as that of the Ni/MS - NH_2/MS catalyst. While, the Ni/MS - NH_2/MS catalyst produced a higher yield of 61.25% showing catalytic synergy that combined the properties of Ni/MS - NH_2/MS, thus enhancing their catalytic performance. Ni/MS is responsible for reducing free fatty acids (FFA), while NH_2/MS optimally converts triglycerides into methyl esters. Additionally, the combined catalyst can offer better stability under reaction conditions and higher selectivity towards methyl ester formation compared to the Ni-NH_2/MS catalyst. This also reduces soap formation and increases methyl ester yield. Furthermore, this is related to a higher ratio of basic/acidic sites compared to the Ni-NH_2/SM catalyst, thus enabling a greater conversion of triglycerides into methyl esters.

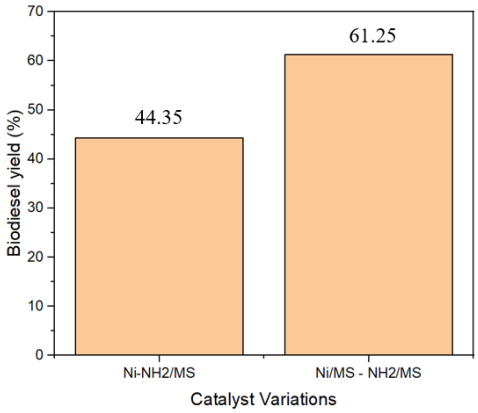

Fig. 8. Effect of catalyst variations on biodiesel yield

3.2.2. Effect of concentration on biodiesel yield

In Fig. 9 based on the research results, a 3% catalyst weight yielded the highest biodiesel conversion. The 3wt% catalyst is effective at most as it provides an optimal activity, accelerating esterification-transesterification reactions without impeding reactions due to catalyst deficiency or excess [32]. While, the 1wt% catalyst, although sufficient to initiate the reaction, exhibited slower reaction rates compared to higher concentrations. Catalysts exceeding 3wt% can cause the catalyst- reactant mixture to be increasingly viscous, leading to increased viscosity that hinders mass transfer processes due to restricted molecular collisions [33]. Therefore, this leads to a decrease in biodiesel yield conversion.

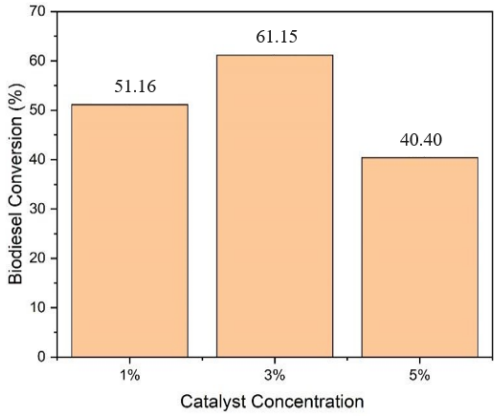

Fig. 9. Effect of catalyst concentration on biodiesel yield

3.2.3. Effect of reaction time on biodiesel yield

A reaction time of 180 minutes (3 hours) indicates the most optimal results in the one-step biodiesel reaction. After 3 hours of reaction, the biodiesel yield continues to decrease until 420 minutes (7 hours) due to the increased contamination or damage to the catalyst. With longer reaction times, the formation of by-products increases, leading to a decrease in biodiesel yield [34,35]. This aligns with the selectivity observed in this study, whereas time increased, the non-methyl ester yields rose from 0.07% to 0.17% at the 420-minute mark. The influence of reaction time on biodiesel conversion can be observed in Fig. 10.

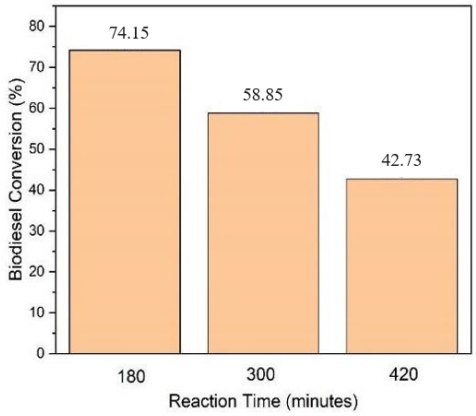

Fig. 10. Effect of reaction time on biodiesel yield

3.2.4. Effect of methanol to oil ratio (MTOR) on biodiesel yield

The molar ratio of oil to alcohol, in this case, methanol, showed an increasing trend with the increasing amount of methanol ratio in the biodiesel activity test (esterification-transesterification) using bifunctional catalysts, as depicted in Fig. 11. In the one-step esterification-transesterification reaction, there is a reaction equilibrium in which, as the methanol to oil ratios increase, the reaction equilibrium can shift to methyl ester formation due to the presence of more methanol to accelerate the reaction [36-38]. As a result, at methanol to oil ratios ranging from 15:1 to 21:1, there is an increase from 44.40% to 75.10%. However, the use of excess methanol is only effective to a certain extent in increasing the conversion of methyl esters [39].

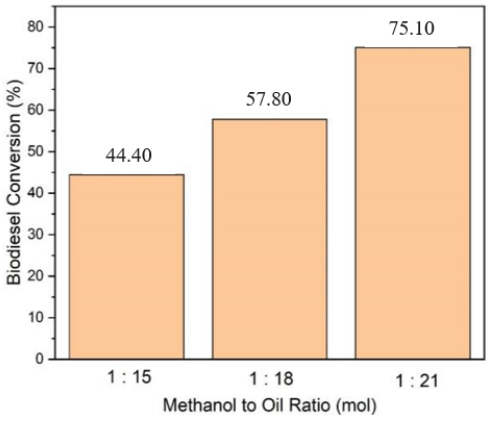

Fig. 11. Effect of methanol to oil ratio on biodiesel yield

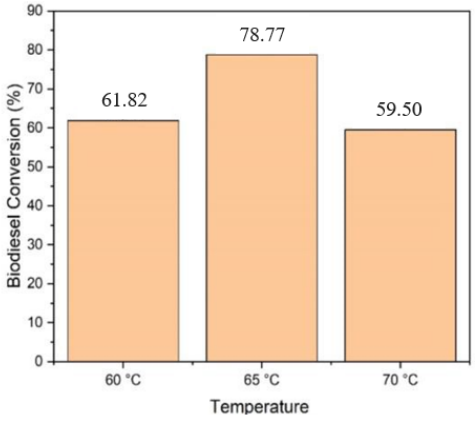

Fig. 12. Effect of reaction temperature on biodiesel yield

3.2.5. Effect of reaction temperature on biodiesel yield

In Fig. 12, at reaction temperatures of 60°C, 65°C, and 70°C, the biodiesel conversions of 61.82%, 78.77%, and 58.49% were respectively obtained. According to the research findings, a temperature of 65°C yielded the highest biodiesel conversion yield consistent with the study conducted by Zein et al. [40] where the maximum conversion of 78.77% was achieved at 65°C. However, the conversion decreased when the temperature was raised to 70°C due to an optimum temperature for the reaction in this study, related to the boiling point of methanol. As the temperature increased above the boiling point of methanol, bubbles formed on the surface, hindering the mass transfer phase, thus resulting in a reduction in biodiesel yield conversion at temperatures above 65°C. The lower temperatures, such as 60°C, will provide insufficient energy for the catalyst to function optimally.

3.3. Biodiesel characterization

3.3.1. GC-MS

The liquid product was obtained from the bifunctional catalysts (Ni/MS - NH2/MS and Ni-NH2/MS) tested for their one-step catalytic activity. The Ni-NH2/MS catalyst yielded 44.35% biodiesel with three main methyl ester components: methyl oleate at 39.96%, methyl palmitate at 37.13%, and methyl linoleate at 13.49%. While, the Ni/MS - NH2/MS

catalyst produced a higher biodiesel yield of 61.25% with the lowest amount of non-methyl ester by-products at only 0.57%. In the Ni/MS - NH2/MS catalyst, a catalytic synergy between Ni/MS and NH2/MS enhanced the catalytic performance due to the higher surface area compared to the Ni-NH2/MS catalyst, as evidenced by surface area analysis results. This then facilitated the interactions between base and acid sites during catalytic activity testing, leading to a more optimal biodiesel yield.

Table 5. FAMEs Composition of The Synthesized Biodiesel

Peaks	Compounds	Molecular Formula	Molecular weight (g/mol)	Retention time (minutes)	Width (%)
1	Methl laurae	$C_{13}H_{26}O_2$	214	24.899	0.2
2	Methyl myristate	$C_{15}H_{30}O_2$	242	29.626	1.4
3	Methyl palmitoleate	$C_{17}H_{32}O_2$	268	33.444	0.3
4	Methyl palmitate	$C_{17}H_{34}O_2$	270	34.063	37.5 37.53
5	Methyl linoleate	$C_{19}H_{34}O_2$	294	37.203	13.6
6	Methyl oleate	$C_{19}H_{36}O_2$	296	37.481	40.5
7	Methyl stearate	$C_{19}H_{38}O_2$	298	37.815	5.6
8	Methyl 10 nonadecenoate	$C_{20}H_{38}O_2$	296	40.852	0.2
9	Methyl arachidate	$C_{21}H_{42}O_2$	326	41.297	0.5

Table 5 provides more detailed information using Ni/MS – NH_2/MS as bifunctional catalyst for one step biodiesel, showing that the methyl esters produced from the optimal esterification-transesterification catalyst comprised 0.22% methyl laurate, 1.394% methyl myristate, 0.25% methyl palmitoleate, 37.53% methyl palmitate, 13.59% methyl linoleate, 40.73% methyl oleate, 5.61% methyl stearate, 0.22% methyl 10-nonadecenoate, and 0.52% methyl arachidate. The three main methyl ester components, with the highest contents, included methyl oleate, methyl palmitate, and methyl linoleate. This finding aligns with previous research by Mahesh et al. [41] who reported that the primary component in biodiesel produced from palm oil waste conversion was methyl oleate. The formation of these methyl esters confirmed that the palm oil waste has been successfully converted into biodiesel.

3.3.2. FTIR

In Fig. 13, a similar wavenumber in waste palm oil and biodiesel was indicated at 3009 cm^{-1}, representing =C-H, absorption bands at 2924 cm^{-1}, and 2854 cm^{-1}, respectively. It represented the symmetric and asymmetric stretching vibrations of CH_3 in –CO-O-CH_3. The characteristic absorption band of the ester carbonyl group (C=O) was observed at 1744 cm^{-1} [42]. Another absorption band at 1458 cm^{-1} represented the vibration of alkane bonds (-C-H). The FTIR spectra of the waste palm oil sample showed a peak at the wavenumber of 1373 cm^{-1}. Peaks in this region indicate the presence of O-CH_2 groups derived from the triglyceride content in the waste palm oil. Absorption at this wavenumber was also observed with lower intensity in the FTIR spectra of products from one-step esterification-transesterification. The peak, which is the vibration of the O-CH_2 group, originated from glycerol, indicating that the product from one-step esterification-transesterification was still contaminated by glycerol due to incomplete separation. Absorption bands at 1165-1242 cm^{-1} represented the stretching vibrations of the (-C-O-) ester groups, while the peak at 725 cm^{-1} represented the rocking plane vibration of –CH_2. The FTIR spectra of biodiesel showed new peaks not detected in the waste palm oil. The characteristic symmetric stretching vibration of C-O-C in biodiesel compounds appeared at the wavenumber of 1018 cm^{-1}. The presence of this peak indicated that the one-step esterification-transesterification reaction has produced biodiesel products.

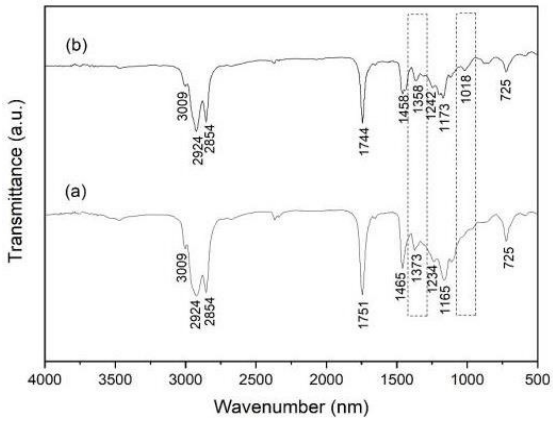

Fig. 13. FTIR spectra of the (a) Waste Palm Oil, and (b) Biodiesel

3.3.3. ^1H NMR analysis

The purpose of 1H NMR analysis is to confirm the results of GC-MS and to determine whether the fatty acids present in the oil have been successfully converted into fatty acid methyl esters (FAME), as indicated by the presence of saturated and unsaturated methyl esters. Fig. 14 presents the ^{1}H-NMR spectrum of biodiesel from waste palm oil.

Fig. 14 shows the characteristic structure of methyl esters visible in the chemical shift pattern at δ = 3.60 ppm with a prominent peak exhibiting a singlet splitting pattern. This peak belongs to the protons of the methoxy (-OCH_3) group in the methyl ester. This methoxy peak is a typical peak of biodiesel appearing at a shift of 3.60 ppm with the integration of 1.00, confirming that the fatty acids in the waste palm oil have been converted into biodiesel. This spectrum also indicated that triglycerides have been converted into methyl esters as no peaks appeared at the chemical shifts of δ= 4.1 ppm and 4.3 ppm. Peaks in this region indicate the presence of triglycerides [43]. Peaks (triplets) at 2.26 ppm and 2.71 ppm represented the α-methylene groups in methyl esters (-CH_2COOMe) and the -

C=CH-CH_2-CH=C- group with integrations of 0.67 and 0.06. The presence of these two peaks also confirms the presence of methyl esters in biodiesel [44]. The singlet peak at 5.29 ppm indicated the presence of alkene groups (-CH=CH-). Peaks with high intensity at 1.20 ppm represented methylene group protons (-(CH_2)n-). Peaks at 1.96 and 1.58 explained the presence of α-methylene proton groups in a double bond (=CH-CH_2-) and β-methylene groups in methyl esters (CH_2-C-CO_2Me), while the triplet peak at 0.81 ppm was terminal methyl protons (C-CH_3). A summary of signals and chemical shifts in ^{1}H NMR is provided in Table 6.

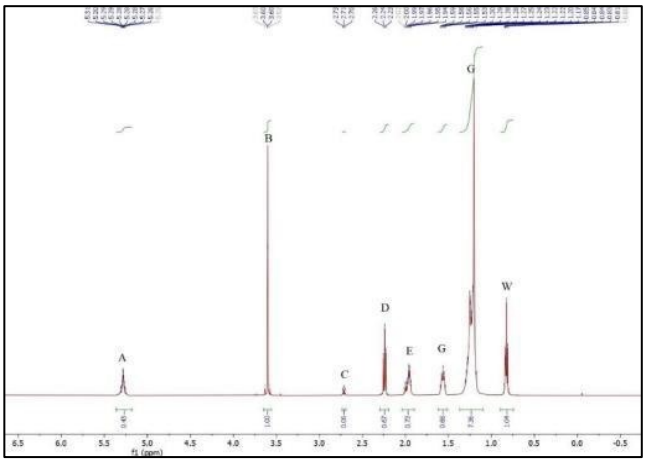

Fig. 14. ^{1}H NMR spectrum of the biodiesel from waste palm oil

The conversion of triglycerides into methyl esters is determined based on the proton integration values of characteristic peaks of biodiesel using Eq. (2). [45]. The percentage conversion of triglycerides into methyl esters corresponding was found to be 99.50%.

3.3.4. ^{13}C NMR analysis

^{13}C NMR analysis in biodiesel characteristic testing aims to provide information on the molecular structure and chemical composition of compounds contained in biodiesel. The ^{13}C NMR spectrum of biodiesel from waste palm oil is shown in Fig. 15.

Table 6. Biodiesel different molecule moieties and their ^{1}H NMR chemical shifts are summarised

Signal	Moietie	Chemical shifts (ppm)
A	-CH = CH-	5.29
B	Methyl Ester –CH_3	3.60
C	-CH_2- between two non-conjugated double	2.71
D	-CH_2- adjacent to to the carbonyl group	2.26
E	-CH_2- adjacent to the double bonds	1.96
G	The aliphatic –CH_2-s	1.20 dan 1.58
W	End of chain aliphatic –Cl	0.81

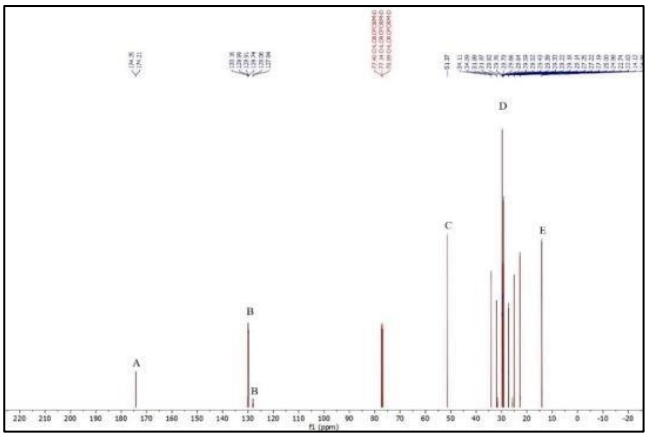

Fig. 15. ^{13}C NMR spectrum of the biodiesel from waste palm oil

Table 7. Biodiesel different molecule moieties and their ^{13}C NMR chemical shifts are summarised

Signal	Moietie	Chemical shifts (ppm)
A	C=O	174.2
B	C=C	130 and 127.9
C	-O-CH_3	51.4
D	-CH_2-	22.6 - 34
E	End of chain -CH_3-	14

The characteristic peaks of carbonyl ester carbon (C=O) were observed at 174.2 ppm, and methyl ester was found at 51.4 ppm. Two peaks at 130 and 127.9 ppm indicated the presence of unsaturation in the fatty acid methyl ester (C=C). Other observed peaks from 22.6 to 34 ppm and 14 ppm were related to the methylene carbons of the methyl ester carbon chain and terminal –CH_3 chains. The chloroform solvent appeared at a peak of around 77.4 ppm. A summary of signals and chemical shifts in ^{13}C NMR is provided in Table 7.

3.4. Reaction mechanism of biodiesel production using bifunctional acid–base catalyst

Fig.16 illustrates the reaction mechanism for biodiesel production using a bifunctional acid-base catalyst. The Ni/MS catalyst acts as an acid site, while the NH_2/MS catalyst acts as a base site. The catalytic reaction involves five steps: reactant diffusion, physical adsorption of reactants, surface reaction, product desorption, and product diffusion. In the first step, the carbonyl group of free fatty acids (FFA) and methanol diffuses from the solution to the catalyst's internal surface through its pores. Then, the FFA carbonyl group is adsorbed on the acidic sites (for esterification), while the methanol molecules are adsorbed on the basic sites (for transesterification) of the catalyst surface. Subsequently, an intermediate is formed by the nucleophilic attack of alcohol on the ester at both the acid and base sites. A hydroxyl group is then released from the intermediate to form one molecule of water and one molecule of fatty acid methyl ester (FAME) on the acid site. On the base site, the C–O bond is broken to produce one molecule of FAME and glycerol as a byproduct. These products are desorbed from the catalyst surface as the reaction progresses. In the final step, all products diffuse from the catalyst surface into the solution, and the cycle repeats for each fatty acid ester [46].

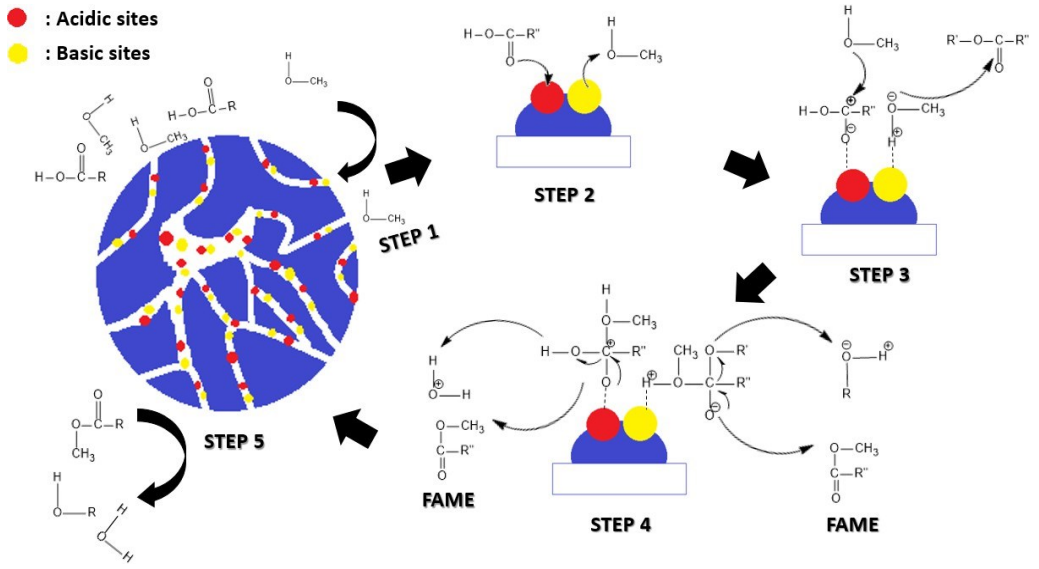

Fig. 16. The Reaction Mechanism of Biodiesel Production Using a Bifunctional Acid–Base Catalyst

3.5. Reusability study

Fig. 17 shows that the performance of the bifunctional Ni/MS - NH_2/MS catalyst remained effective up to three cycles with only a slight decrease in biodiesel yield. The highest biodiesel conversion was achieved in the first reaction at 74.64%. In the second and third cycles, the conversion decreased slightly to 72.44% and 72.00%, respectively. This decline in performance was likely due to the adsorption of biodiesel products onto the catalyst surface, hindering the interaction of fresh reactants with the active sites of the catalyst [49-51]. Despite this, the catalyst still maintained relatively high conversion rates after three cycles, indicating that it can be reused effectively without any significant loss in performance. Additionally, the decrease in conversion rate over successive cycles was not drastic, suggesting that the catalyst exhibited good stability and reusability. This made the process more cost-effective in terms of material usage and more environmentally friendly, as the catalyst could be regenerated and reused without the need for large quantities of fresh catalyst for each cycle.

3.6. Comparing Ni/MS – NH_2/MS catalyst with previously reported catalysts

As shown in Table 8, the current Ni/MS – NH_2/MS catalyst was compared with different in the specific context of WPO conversion to FAME. This study demonstrated advantages in terms of effectiveness, both in the conversion of vegetable oil to biodiesel and in achieving more efficient reaction conditions. The use of natural-based catalysts, such as Ni/MS - NH_2/MS, was more cost-effective compared to more complex catalysts like GO-KOH-Kaolinit, which could lower biodiesel production costs. Additionally, high biodiesel yields were achieved in shorter reaction times under more environmentally friendly and cost-effective conditions. The use of waste palm oil as a feedstock and Ni/MS - NH_2/MS as a catalyst shows great potential for economically and ecologically sustainable biodiesel production.

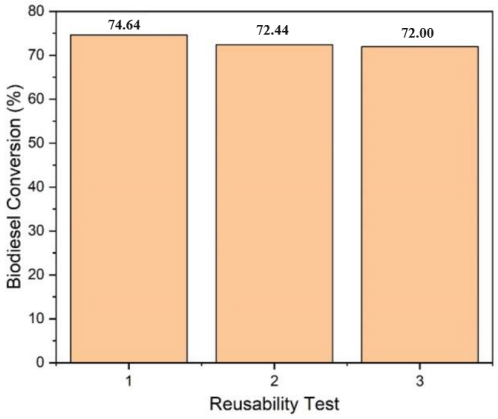

Fig. 17. Effect of reusability test catalyst on biodiesel yield

Table 8. Comparison of Ni/MS - NH_2/SM Catalysts with Previous Studies

Catalyst	Feed	Biodiesel Yield (%)	Reaction Conditions	References
SrO/MgO	Palm oil	47.17	5% wt catalyst; 60 °C; 2 hours; methanol to oil ratio 9:1	[47]
GO-KOH-Kaolinit	Waste palm Oil	58	5% wt catalyst; 60 °C; 4 hours; methanol to oil ratio 6:1	[48]
NH_2/MCM 41	Waste palm Oil	76.55	-	[18]
Ni/MS - NH_2/MS	Waste palm Oil	78.77	3% wt catalyst; 65 °C; 3 hours; methanol to oil ratio 21:1	This research

4. Conclusion

This study demonstrates that Sidoarjo mud can be utilized as a renewable resource for producing bifunctional catalysts. Two types of bifunctional catalysts, Ni/MS - NH_2/MS and Ni-NH_2/MS, were successfully synthesized. The combined catalyst, Ni/MS - NH_2/MS, enabled simultaneous esterification and transesterification one step under mild conditions, achieving the highest biodiesel yield. The maximum biodiesel yield obtained was 78.77% under optimal reaction conditions wt% Ni/MS - NH_2/MS, methanol to oil ratio 21:1, temperature reaction 65°C, and time reaction 180 minutes. The catalyst remained effective for at least three reuse cycles, maintaining a conversion level of approximately 72%. The results also confirmed the successful characterization and identification of biodiesel components' molecular structures using GCMS, ^{1}H NMR and ^{13}C NMR. This in-depth investigation of silica-based catalysts, particularly Ni/MS - NH_2/MS, provides valuable insights for optimizing conditions to produce biodiesel efficiently and sustainably, contributing to the development of catalysts with enhanced performance and stability in the biodiesel production process.

Acknowledgements

Flagship research grant funding with agreement decree number 2458/UN1/FMIPA.1.3/KP/PT.01.03/2024. Also, the Center for Higher Education Funding (BPPT), and Indonesia Endowment Fund for Education (LPDP) and facility from Universitas Gadjah Mada.

References

1. A.F.H. Soegiharto, *The role of flue gas inhibitor on stabilizing heptane flame in meso scale combustor*, J. Energy Mech. Mater. Manuf. Eng. 111 (2021) 111–118.
2. Y. Mao, J. Cheng, H. Guo, L. Qian, W. Yang, J.Y. Park, *Synthesis of acid–base bifunctional catalysts by in situ growth of Co-LDH nanosheets on HY zeolite to enhance Co(OH)x utilization for microalgal lipid conversion*, Energy Fuels 37 (2023) 5220–5228.
3. O.E. Ajala, F. Aberuagba, T.E. Odetoye, A.M. Ajala, *Biodiesel: sustainable energy replacement to petroleum-based diesel fuel—a review*, ChemBioEng Rev. 2 (2015) 145–156.
4. B. Tabah, A.P. Nagvenkar, N. Perkas, A. Gedanken, *Solar-heated sustainable biodiesel production from waste cooking oil using a sonochemically deposited SrO catalyst on microporous activated carbon*, Energy Fuels 31 (2017) 6228–6239.
5. X. Liu, H. He, Y. Wang, S. Zhu, X. Piao, *Transesterification of soybean oil to biodiesel using CaO as a solid base catalyst*, Fuel 87 (2008) 216–221.
6. L. Du, Z. Li, S. Ding, C. Chen, S. Qu, W. Yi, J. Ding, *Synthesis and characterization of carbon-based MgO catalysts for biodiesel production from castor oil,* Fuel 258 (2019) 116122.
7. D. Ganesan, A. Rajendran, V. Thangavelu, *An overview on the recent advances in the transesterification of vegetable oils for biodiesel production using chemical and biocatalysts*, Rev. Environ. Sci. Biotechnol. 8 (2009) 367–394.
8. D. Srinivas, J.K. Satyarthi, *Biodiesel production from vegetable oils and animal fat over solid acid double-metal cyanide catalysts*, Catal. Surv. Asia 15 (2011) 145–160.
9. D. Faria, F. Santos, G. Machado, R.V. Lourega, P. Eichler, G. De Souza, J. Lima, *Extraction of radish seed oil (Raphanus sativus L.) and evaluation of its potential in biodiesel production*, AIMS Energy 6(4) (2018) 551-565.
10. D. Singh, D. Sharma, S.L. Soni, S. Sharma, D. Kumari, *Chemical compositions, properties, and standards for different generation biodiesels: a review*, Fuel 253 (2019) 60–71.
11. H. Zhang, H. Li, Y. Hu, K.T.V. Rao, C.C. Xu, S. Yang, *Advances in production of bio-based ester fuels with heterogeneous bifunctional catalysts*, Renew. Sustain. Energy Rev. 114 (2019) 109296.
12. Al-Saadi, B. Mathan, Y. He, *Esterification and transesterification over SrO–ZnO/Al_2O_3 as a novel bifunctional catalyst for biodiesel production*, Renew. Energy 158 (2020) 388–399.
13. V. Enguilo Gonzaga, R. Romero, R.M. Gómez-Espinosa, A. Romero, S.L. Martínez, R. Natividad, *Biodiesel production from waste cooking oil catalyzed by a bifunctional catalyst*, ACS Omega 6 (2021) 24092–24105.
14. H. Noureddini, D. Harkey, V. Medikonduru, *A continuous process for the conversion of vegetable oils into methyl esters of fatty acids*, JAOCS, J. Am. Oil Chem. Soc. 75 (1998) 1775–1783.
15. B. Changmai, C. Vanlalveni, A.P. Ingle, R. Bhagat, L. Rokhum, *Widely used catalysts in biodiesel production: a review*, RSC Adv. 10 (2020) 41625–41679.
16. D. Zhao, Q. Huo, J. Feng, J. Kim, Y. Han, G.D. Stucky, *Novel mesoporous silicates with two-dimensional mesostructure direction using rigid bolaform surfactants*, Chem. Mater. 11 (1999) 2668–2672.
17. C. Hsu, H.P.L. Tang, C. Lin, *Synthesis of mesoporous silica and mesoporous carbon using gelatin as organic template*, Stud. Surf. Sci. Catal. 165 (2007) 385–388.
18. Ifah, W. Trisunaryanti, Triyonno, K. Dewi, *Synthesis of MCM-41- NH_2 catalyst by sonochemical method for transesterification of waste palm oil*, Int. J. ChemTech 9 (2016) 382–387.
19. T. Triyono, H.M. Khoiri, W. Trisunaryanti, K. Dewi, *Synthesis of NH_2/MCM-41 catalysts using silica from Sidoarjo mud and their characterization for palm oil transesterification*, IOSR J. Appl. Chem. 8 (2015) 50–56.
20. H.I.M. Ortiz, Y.P. Mercado, J.A.M. Silva, Y.O. Maldonado, G. Castruita, L.A.G. Cerda, *Functionalization with amine-containing organosilane of mesoporous silica MCM-41 and MCM-48 obtained at room temperature*, Ceram. Int. 40 (2014) 9701–9707.
21. M. Ulfa, W. Trisunaryanti, I.I. Falah, I. Kartini, I. Sutarno, *Synthesis of mesoporous carbon using gelatin as a source of carbon by hard template technique and its characterizations*, IOSR J. Appl. Chem. 4 (2014) 1–7.
22. S.A. Kadapure, P. Kirti, S. Singh, S. Kokatnur, N. Hiremath, A. Variar, et al., *Studies on process optimization of biodiesel production from waste cooking and palm oil*, Int. J. Sustain. Eng. 11 (2018) 167–172.
23. W. Trisunaryanti, A. Alethiana, I.I. Falah, D.A. Fatmawati, *Effective production of biofuel from used cooking oil over Ni–Pd loaded on amine-functionalized Lapindo Mud catalyst*, React. Kinet. Mech. Catal. 135 (2022) 951–970.
24. D. Hardjito, Antoni, G.M. Wibowo, D. Christianto, Pozzolanic *activity assessment of LUSI mud in semi high volume pozzolanic mortar*, Mater. 5 (2012) 1654–1660.
25. W. Trisunaryanti, A. Syofian, S. Purwono, *Characterization and modification of Indonesia natural zeolite for hydrocracking of waste lubricant oil into liquid fuel fraction*, J. Chem. Eng. 7 (2013) 175–180.
26. T. Triyono, H.M. Khoiri, W. Trisunaryanti, K. Dewi, *Synthesis of NH_2/MCM-41 catalysts using silica of Sidoarjo mud and their*

characterization for palm oil transesterification, IOSR J. Appl. Chem. 8 (2015) 50–56.

27. L. Travaglini, P. Picchetti, A. Del Giudice, L. Galantini, L. De Cola, *Tuning and controlling the shape of mesoporous silica particles with CTAB/sodium deoxycholate catanionic mixtures*, Microporous Mesoporous Mater. 279 (2019) 423–431.
28. M. Alsaiari, B.T.T. Thao, N.H. Hieu, N.P.H. Duy, D.V.N. Vo, T. Witoon, A. Al-Gheethi, *High selective hydrocarbon and hydrogen products from catalytic pyrolysis of rice husk: role of the ordered mesoporous silica derived from rice husk ash for Ni-nanocatalyst performance*, J. Anal. Appl. Pyrolysis 178 (2024) 106383.
29. N.M. Popova, L.A. Sokolova, E.A. Marchenko, L.N. Bobrova, *TPD study of NH_3 adsorption/desorption on the surface of V/Ti, V/Al based catalysts for selective catalytic reduction of NO_x by ammonia. TPD test of γ-Al_2O_3, TiO_2 (anatase) and alumina- supported vanadia catalysts*, React. Kinet. Catal. Lett. 65 (1998) 363–370.
30. T. Yan, W. Bing, M. Xu, Y. Li, Y. Yang, G. Cui, M. Wei, *Acid– base sites synergistic catalysis over Mg–Zr–Al mixed metal oxide toward synthesis of diethyl carbonate*, RSC Adv. 8 (2018) 4695– 4702.
31. J. Prameswari, W. Widayat, L. Buchori, H. Hadiyanto, *Novel iron sand-derived α-Fe_2O_3/CaO_2 bifunctional catalyst for waste cooking oil-based biodiesel production*, Environ. Sci. Pollut. Res. 30 (2023) 98832–98847.
32. W. Wendi, *Effect of Reaction Temperature and Catalyst Concentration*, in: Sriwijaya Int. Semin. Energy-Environ. Sci. Technol., Vol. 1, No. 1, 2014, pp. 32–37.
33. U.L. Azzahro, W. Broto, *Utilization of Waste Shells as CaO Catalyst in Biodiesel Production from Used Cooking Oil*, Acta Chim. Asiana 5 (2022) 147–152.
34. P.M. Anisah, E. Agustian, *Effect of transesterification on the result of waste cooking oil conversion to biodiesel*, J. Phys.: Conf. Ser. 1170 (2019) 012067, IOP Publishing.
35. N. Kolesárová, M. Hutňan, I. Bodík, V. Špalková, *Utilization of biodiesel by-products for biogas production*, BioMed Res. Int. 2011 (2011).
36. M.D. Supardan, S. Satriana, M. Mahlinda, *Biodiesel production from waste cooking oil using hydrodynamic cavitation*, Makara J. Technol. 16 (2012) 10.
37. N.S.M. Alias, H. Veny, F. Hamzah, N. Aziz, *Effect of free fatty acid pretreatment to yield, composition and activation energy in chemical synthesis of fatty acid methyl ester, Indones*. J. Chem. 19 (2019) 592–598.
38. H. Jabbari, *Production of methyl ester biofuel from sunflower oil via transesterification reaction*, Asian J. Nanosci. Mater. 1 (2018) 52–55.
39. D.A. Ramdhani, W. Trisunaryanti, *Study of green and sustainable heterogeneous catalyst produced from Javanese Moringa oleifera leaf ash for the transesterification of Calophyllum inophyllum seed oil,* Commun. Sci. Technol. 8 (2023) 124–133.
40. Y.M. Zein, A.K. Anal, D. Prasetyoko, I. Qoniah, *Biodiesel production from waste palm oil catalyzed by hierarchical ZSM-5 supported calcium oxide,* Indones. J. Chem. 16 (2016) 98–104.
41. S.E. Mahesh, A. Ramanathan, K.M.S. Begum, A. Narayanan, *Biodiesel production from waste cooking oil using KBr impregnated CaO as catalyst*, Energy Convers. Manag. 91 (2015) 442–450.
42. S. O'Donnell, I. Demshemino, M. Yahaya, I. Nwadike, L. Okoro, *A review on the spectroscopic analyses of biodiesel*, Eur. Int. J. Sci. Technol. 2 (2013) 137–146.
43. M. Tariq, S. Ali, N. Muhammad, N.A. Shah, M. Sirajuddin, M.N. Tahir, M.R. Khan, *Biological screening, DNA interaction studies, and catalytic activity of organotin(IV) 2-(4-ethylbenzylidene) butanoic acid derivatives: synthesis, spectroscopic characterization, and X-ray structure*, J. Coord. Chem. 67 (2014) 323–340.
44. R. Aitbelale, I. Abala, F.E.M.H. Alaoui, A. Sahibed-dine, N.M. Rujas, F. Aguilar, *Characterization and determination of thermodynamic properties of waste cooking oil biodiesel: Experimental, correlation and modeling density over a wide temperature range up to 393.15 and pressure up to 140 MPa*, Fluid Phase Equilib. 497 (2019) 87–96.
45. M. Tariq, S. Ali, F. Ahmad, M. Ahmad, M. Zafar, N. Khalid, M.A. Khan, *Identification, FT-IR, NMR (^{1}H and ^{13}C) and GC/MS studies of fatty acid methyl esters in biodiesel from rocket seed oil,* Fuel Process. Technol. 92 (2011) 336–341.
46. N.J.A. Rahman, A. Ramli, K. Jumbri, Y. Uemura, *Tailoring the surface area and the acid–base properties of ZrO_2 for biodiesel production from Nannochloropsis sp.,* Sci. Rep. 9 (2019) 1–12.
47. D.J. Qoyima, *Modification of Magnesium Oxide from Bittern Waste with Strontium Oxide for Palm Oil Transesterification Process,* Indones. J. Chem. Sci. 10 (2021) 2.
48. S. Syukri, F. Ferdian, Y. Rilda, Y.E. Putri, M. Efdi, U. Septiani, *Synthesis of graphene oxide enriched natural kaolinite clay and its application for biodiesel production*, Int. J. Renew. Energy Dev. 10 (2021) 307–315.
49. N. Oueda, Y.L. Bonzi-Coulibaly, I.W. Ouédraogo, *Deactivation processes, regeneration conditions and reusability performance of CaO or MgO based catalysts used for biodiesel production*—a review, Mater. Sci. Appl. 8 (2016) 94–122.
50. M.R. Bayramoğlu, İ. Korkut, B.T. Ergan, *Reusability and regeneration of solid catalysts used in ultrasound-assisted biodiesel production*, Turk. J. Chem. 45 (2021) 342–347.
51. Istadi, U. Mabruro, B.A. Kalimantini, L. Buchori, D.D. Anggoro, *Reusability and stability tests of calcium oxide-based catalyst (K_2O/CaO-ZnO) for transesterification of soybean oil to biodiesel*, Bull. Chem. React. Eng. Catal. 11 (2016) 34–39.